



# Facile strategy for uniform gold coating on silver nanowires embedded PDMS for soft electronics



Haechan Park <sup>1</sup>, Sehyun Kim<sup>1</sup>, Juyeong Lee<sup>1</sup>, Kwangmin Kim<sup>1</sup>, Hanah Na <sup>2</sup>, Yeeun Kim<sup>1</sup>, Daeun Kim<sup>1</sup>, Donghyung Shin<sup>1</sup>, BongSoo Kim<sup>1,3,4</sup> & Kyoseung Sim <sup>1,5</sup>

Silver nanowires-embedded polydimethylsiloxane (AgNWs/PDMS) electrodes are promising components for various soft electronics, but face energy mismatch with organic semiconductors. Attempts at galvanic replacement, involving spontaneous gold (Au) formation on the electrodes, often result in non-uniform and particulate Au coatings, compromising device performance and stability. In this study, we introduce a novel approach for achieving a uniform and complete Au coating on AgNWs/PDMS electrodes by adding NaCl to the Au complex solution. This addition slows down the galvanic replacement process and prevents precipitation, enabling a uniform and complete Au coating on the AgNWs surface. Such coating significantly reduces contact resistance ( $R_C$ ), thereby enhancing the electrical characteristics of *p*-type organic transistors. Furthermore, the development of high-performance, fully soft organic transistors was achieved incorporating an organic semiconductor-elastomer blend. Additionally, reliable, mechanically stable soft glucose sensor was developed, taking advantage of the complete Au coating, which protects against oxidation during the glucose sensing process.

Recent interest in wearable electronics has intensified due to its promising potential for practical usability<sup>1-4</sup>. Many advancements, including structural engineering and innovative material design, have paved the way for soft electronics, such as skin-mountable and bio-implantable devices<sup>3-7</sup>. Particularly, studies in intrinsically stretchable electronic materials and rubbery composites have played a crucial role in developing fully soft organic electronic devices that enable intimate mounting on skin or implanting into the human body<sup>3,6,7</sup>. While such material development has been a primary focus, the interface between components is indeed critical for the significant advancement of high-performance fully soft organic electronics<sup>8-10</sup>. The contact resistance ( $R_C$ ), mainly induced by the difference between Fermi levels ( $E_F$ ) of metal electrodes and energy levels of semiconductors, obstructs charge carrier transport at the interface, hampering field-effect mobility in organic transistors<sup>9,10</sup>. However, interfacial engineering for minimizing  $R_C$  in fully soft organic transistors has been overlooked, although efforts in reducing it for rigid and flat transistors have been studied<sup>8,11,12</sup>, which is not compatible with devices that are made out of only soft components. Thus,

there is an urgent need in the development of the appropriate approach to form better interface for fully soft organic electronics.

The recently developed fully soft organic transistors, which employ silver nanowires-embedded PDMS (AgNWs/PDMS) as a soft electrode, are promising due to their exceptional electrical and mechanical properties. However, they face an inherent challenge regarding the energy barrier between silver ( $E_{F,Ag}$  is from  $-4.26$  eV), and typical *p*-type organic semiconductors ( $E_{HOMO}$  is from  $-4.90$  to  $-5.50$  eV)<sup>13,14</sup>. A common solution, the galvanic replacement of the AgNWs surface with gold ( $E_{F,Au}$  is  $-5.09$  eV), ensures ohmic contact between soft electrodes and the organic semiconductor<sup>15-17</sup>. Nonetheless, this method often leads to non-uniform gold particulation on AgNWs due to the vigorous redox reaction<sup>18,19</sup>. Particularly, incomplete gold coverage and a rough surface can result in a large  $R_C$  in soft transistors<sup>19</sup>. Moreover, inconsistent gold coverage on AgNWs within the AgNWs/PDMS electrodes limits their application in soft biosensors due to the chemical instability of silver<sup>20</sup>. Therefore, a more

<sup>1</sup>Department of Chemistry, Ulsan National Institute of Science and Technology (UNIST), Ulsan, 44919, Republic of Korea. <sup>2</sup>Center for Advanced Specialty Chemicals, Korea Research Institute of Chemical Technology (KRICT), Ulsan, 44412, Republic of Korea. <sup>3</sup>Graduate School of Semiconductor Materials and Device Engineering, Ulsan National Institute of Science and Technology (UNIST), Ulsan, 44919, Republic of Korea. <sup>4</sup>Graduate School of Carbon Neutrality, Ulsan National Institute of Science and Technology (UNIST), Ulsan, 44919, Republic of Korea. <sup>5</sup>X-Dynamic Research Center, Ulsan National Institute of Science and Technology (UNIST), Ulsan, 44919, Republic of Korea. e-mail: [kyos@unist.ac.kr](mailto:kyos@unist.ac.kr)

promising approach would involve achieving a complete and uniform gold coating through a simple process.

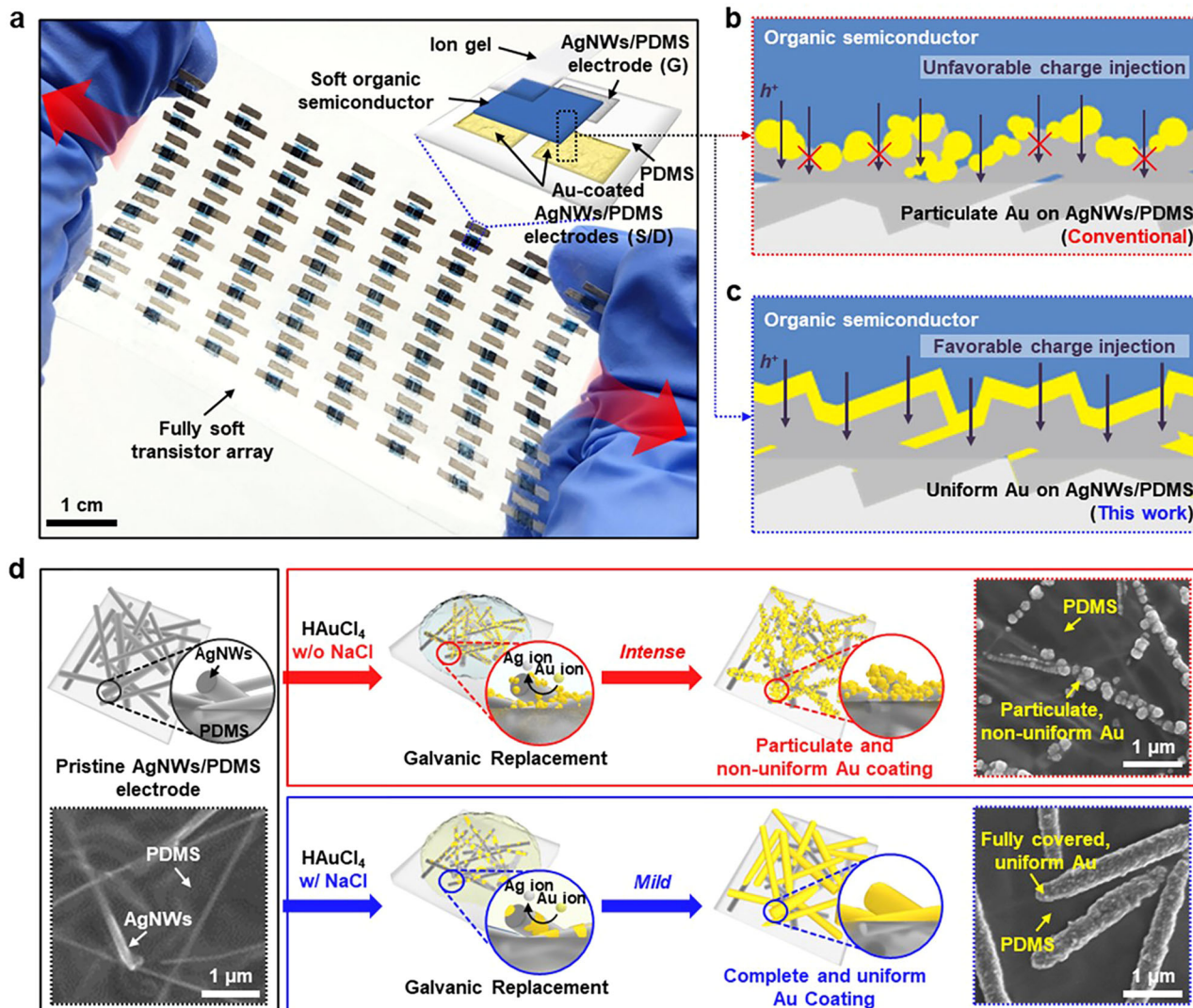
In this study, we report an effective approach for gold coating on exposed AgNWs in AgNWs/PDMS electrodes, aimed at reducing the  $R_C$  in fully soft organic transistors. The key concept in this approach is the controlled deceleration of the galvanic replacement reaction, achieved by employing  $\text{HAuCl}_4$  solution with added  $\text{NaCl}$ . The excess  $\text{Cl}^-$  ions, dissociated from  $\text{NaCl}$ , play a crucial role in moderating the redox reaction according to Le Chatelier's principle, reducing the reduction potential difference, and preventing  $\text{AgCl}$  precipitation. Although many studies have reported on the effects of  $\text{NaCl}$  in galvanic replacement, none have applied these findings to soft electronics; instead, most have all focused on the formation of nano-sized materials<sup>21–23</sup>. This study revealed a direct correlation between the concentration of  $\text{NaCl}$  ( $C_{\text{NaCl}}$ ) in the  $\text{HAuCl}_4$  solution and various properties, including the quality of gold coating,  $R_C$ , and  $\mu_{\text{FE}}$  of the transistor. Significantly, our approach of achieving a uniform gold coating on AgNWs led to a substantial reduction in  $R_C$ , thus accomplishing the high-performance fully soft organic transistors, with an average mobility of  $13.09 \text{ cm}^2 \cdot \text{V}^{-1} \cdot \text{s}^{-1}$ , and the highest mobility of  $21.87 \text{ cm}^2 \cdot \text{V}^{-1} \cdot \text{s}^{-1}$ . Furthermore, the uniform and reliable gold coating on AgNWs of AgNWs/PDMS has shown further advantages in enzyme-based soft glucose sensors,

particularly by offering enhanced chemical resistance to  $\text{H}_2\text{O}_2$ , thereby ensuring reliable sensing capability.

## Results

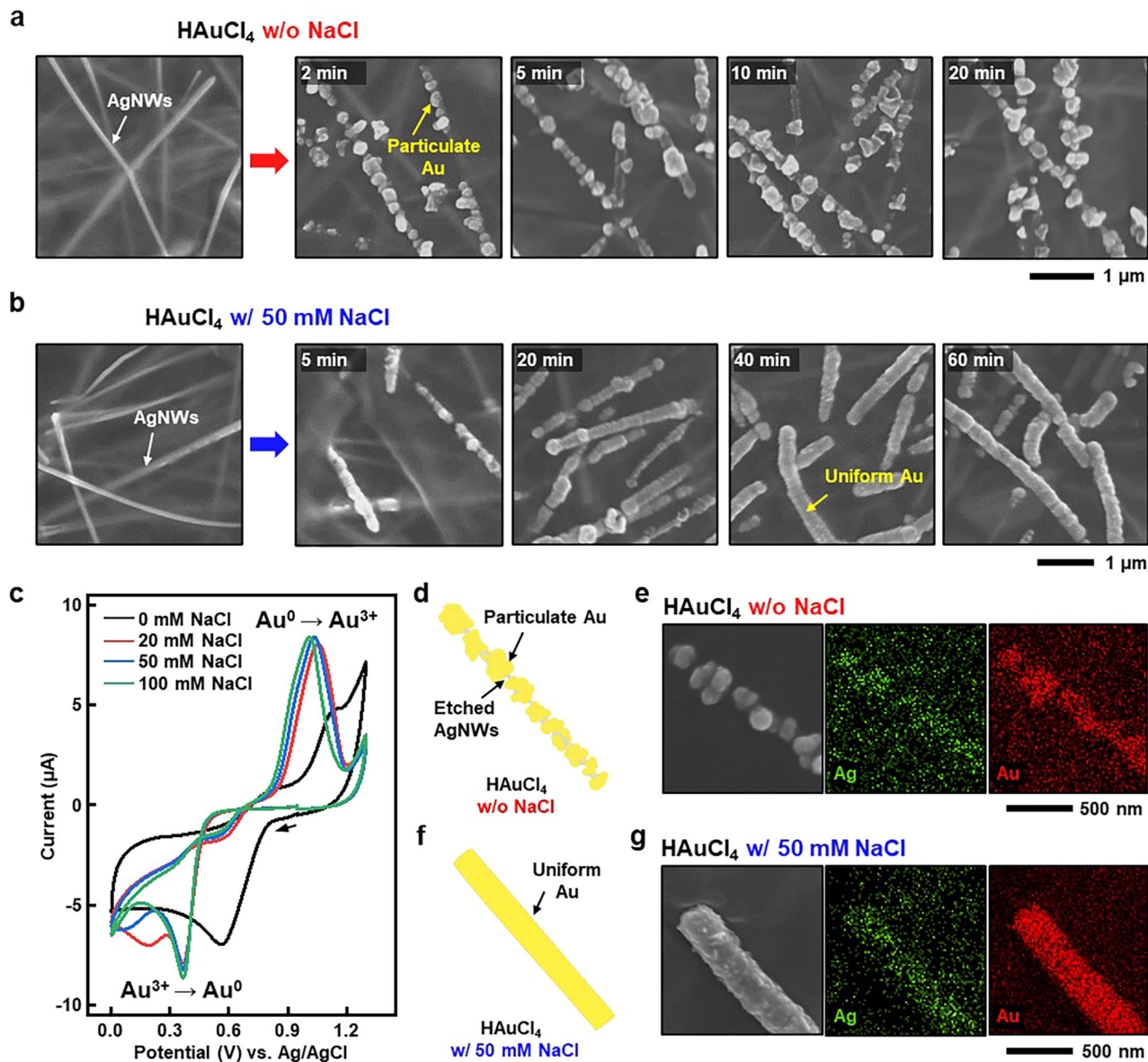
### Au-coated AgNWs/PDMS soft electrodes for soft organic transistors

Figure 1a shows an  $8 \times 8$  array of fully soft organic transistors fabricated using Au-coated AgNWs/PDMS source, drain electrodes, an AgNWs/PDMS gate electrode, a soft organic semiconductor, and ion gel dielectrics. Conventional Au deposition on AgNWs/PDMS typically leads to unfavorable charge transport between the organic semiconductor and soft electrodes, as shown in Fig. 1b. In contrast, a uniform Au coating on AgNWs/PDMS enables efficient charge transport (Fig. 1c), thereby reducing  $R_C$  and enhancing device performance, such as charge carrier mobility. Therefore, achieving uniform Au coating on AgNWs/PDMS is crucial for the high performance of fully soft organic transistors. Figure 1d schematically illustrates the galvanic replacement process for Au coating on the exposed AgNWs of AgNWs/PDMS electrodes, comparing the use of  $\text{HAuCl}_4$  solution with and without  $\text{NaCl}$ . The preparation of AgNWs/PDMS electrodes is detailed in the Experimental Section. The



**Fig. 1 | Au-coated AgNWs/PDMS soft electrodes prepared by galvanic replacement.** **a** An optical image of the  $8 \times 8$  fully soft organic transistors array. Inset is the schematic exploded view of the single fully soft organic transistor. **b, c** Schematic of the charge injection between the organic semiconductor and particulate Au-coated

AgNWs/PDMS electrodes (**b**), and uniform Au-coated AgNWs/PDMS electrodes (**c**). **d** Schematic of the galvanic replacement process of AgNWs/PDMS electrodes using  $\text{HAuCl}_4$  solution in the presence and absence of  $\text{NaCl}$ . Insets are SEM images of the soft electrode under each condition.



**Fig. 2 | Reaction kinetics of Au coating process.** Time-dependent SEM images of the Au-coated AgNWs/PDMS electrodes prepared by galvanic replacement using 0.5 mM HAuCl<sub>4</sub> solution without NaCl (a), and with 50 mM NaCl (b). c Cyclic voltammograms of 0.5 mM HAuCl<sub>4</sub> solution without, and with various

concentrations of NaCl. Schematic of the Au-coated AgNWs/PDMS electrodes using 0.5 mM HAuCl<sub>4</sub> solution without NaCl (d), and with 50 mM NaCl (f). EDS elements mapping of the Au-coated AgNWs/PDMS electrodes using 0.5 mM HAuCl<sub>4</sub> solution without NaCl (e) and with 50 mM NaCl (g).

conventional Au coating via galvanic replacement using HAuCl<sub>4</sub> solution results in an intense reaction that creates a particulate and non-uniform Au layer, whereas the inclusion of NaCl in the solution facilitates a uniform and complete coverage of Au on AgNWs/PDMS electrodes, as shown in the insets of the scanning electron microscopic (SEM) images in Fig. 1d. The detailed kinetics of the NaCl effect on the galvanic replacement process for the soft electrode will be discussed in the following section.

#### The effect of NaCl on Au coating of soft AgNWs/PDMS electrodes

Figure 2a, b exhibit SEM images of exposed AgNWs of AgNWs/PDMS electrodes over time during the galvanic replacement process, comparing the use of HAuCl<sub>4</sub>-only solution and the solution containing 50 mM NaCl. In the case of the galvanic replacement with the HAuCl<sub>4</sub>-only solution, no significant change was observed after 2 min, suggesting rapid reaction completion, and resulting in particulate and non-uniform Au coating on AgNWs. On the other hand,

the HAuCl<sub>4</sub> solution containing 50 mM NaCl completed the reaction in approximately 40 min, achieving uniform Au coverage. It is noted that the NaCl concentration ( $C_{\text{NaCl}}$ ) in the HAuCl<sub>4</sub> solution is optimized at 50 mM due to negligible changes at higher concentrations, as shown in Supplementary Fig. 1. In addition, NaCl does not cause corrosion or structural damage to the AgNWs/PDMS electrode during the galvanic replacement because the short treatment period is not sufficient to have an adverse effect on the AgNWs (Supplementary Fig. 2). Optical microscopic (OM) images also corroborate that complete and uniform Au coverage is saturated at the  $C_{\text{NaCl}}$  of 50 mM (Supplementary Fig. 3). Importantly, HAuCl<sub>4</sub> concentration ( $C(\text{HAuCl}_4)$ ) does not impact the Au coating on AgNWs even after 60 min, as shown in Supplementary Fig. 4, underscoring the critical role of NaCl in achieving uniform Au formation on AgNWs.

The mechanism for uniform Au coating using HAuCl<sub>4</sub> with NaCl is attributed to two key phenomena: (1) slowed reaction rate from Le Chatelier's principle and a negative shift in reduction potential, and (2)

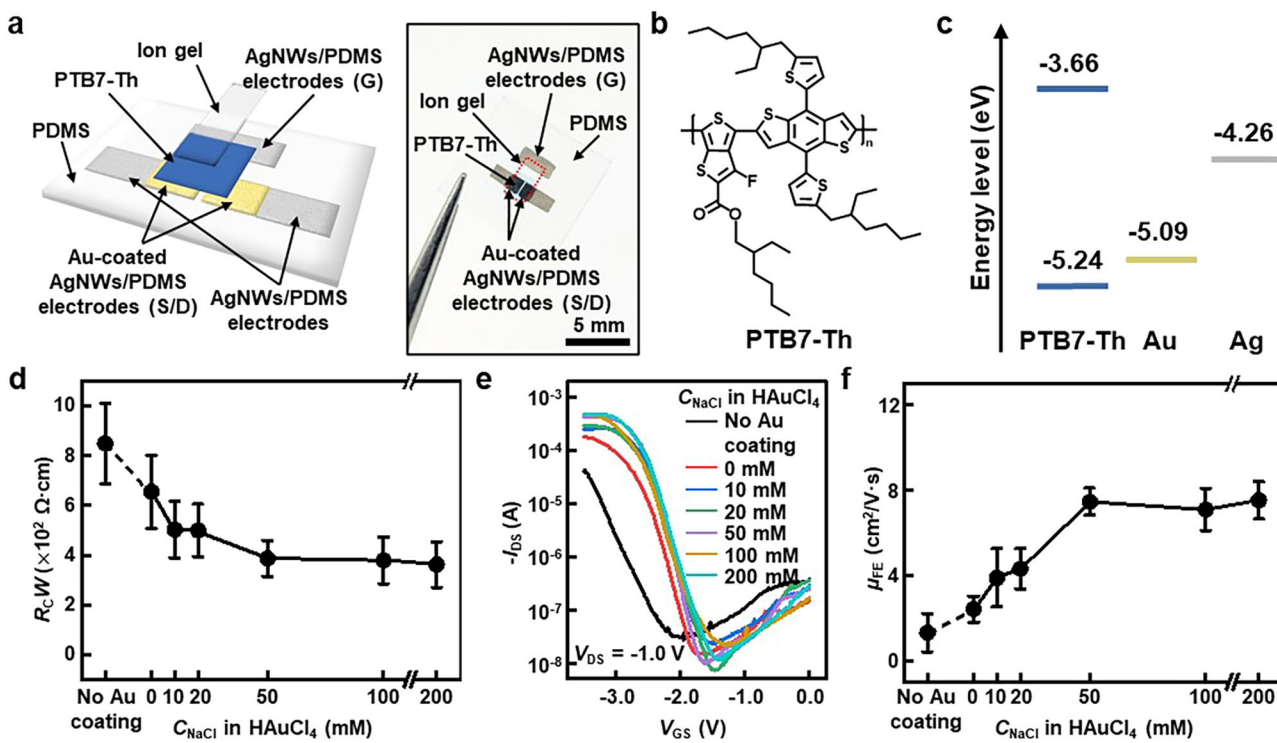
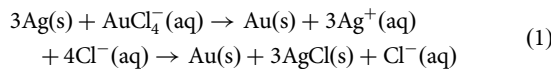


**Fig. 3 | Characterization of Au-coated AgNWs/PDMS electrodes-based *p*-type organic transistors.** **a**, Schematic exploded view (left), and an optical image (right) of the Au-coated AgNWs/PDMS electrodes-based *p*-type organic transistor. **b** A molecular structure of PTB7-Th. **c** Energy levels of the PTB7-Th, gold, and silver. **d**  $R_C W$  of the organic transistors prepared using 0.5 mM HAuCl<sub>4</sub> solution varying  $C_{\text{NaCl}}$ . Data are presented as mean values  $\pm$  1 standard deviation (s.d.) based on

measurements from 30 devices. **e** Representative transfer characteristics of the organic transistors based on the Au-coated AgNWs/PDMS electrodes prepared using 0.5 mM HAuCl<sub>4</sub> solution varying  $C_{\text{NaCl}}$ . **f** The calculated  $\mu_{\text{FE}}$  of the organic transistors based on the Au-coated AgNWs/PDMS electrodes prepared using 0.5 mM HAuCl<sub>4</sub> solution varying  $C_{\text{NaCl}}$ . Data are presented as mean values  $\pm$  1 s.d. based on measurements from 10 devices.

prevention of AgCl precipitation through soluble complex formation. The reaction, driven by the reduction potential difference between AuCl<sub>4</sub><sup>-</sup> and Ag<sup>+</sup>, is described by equation (1):



In the presence of NaCl, excess Cl<sup>-</sup> shifts the equilibrium leftward by Le Chatelier's principle, slowing the galvanic replacement reaction<sup>24,25</sup>. In addition, the reduction potential difference between AuCl<sub>4</sub><sup>-</sup>/Au<sup>0</sup> and Ag<sup>+</sup>/Ag<sup>0</sup> is closely related to the reaction rate<sup>18</sup>. As shown in the cyclic voltammogram in Fig. 2c, the cathodic scan reveals a peak at 0.56 V versus Ag/AgCl for reduction to Au<sup>0</sup>, shifting to 0.35 V with 50 mM NaCl, indicating a reduced galvanic replacement driving force. Interestingly, while  $C_{\text{NaCl}}$  does not significantly affect the reduction potential of AuCl<sub>4</sub><sup>-</sup>/Au<sup>0</sup>, anodic peaks shift negatively with higher  $C_{\text{NaCl}}$ , implying easier oxidation of Au<sup>0</sup> and equilibrium shift towards AuCl<sub>4</sub><sup>-</sup> formation. Furthermore, AgCl precipitation intensifies particulate Au formation<sup>19</sup>, mitigated by soluble Ag complex (AgCl<sub>2</sub><sup>-</sup>) formation in excess Cl<sup>-</sup> conditions<sup>19,26</sup>, as evidenced by energy dispersive X-ray spectroscopy (EDX) analysis showing concentrated Cl distribution on particulate Au (Supplementary Fig. 5).

The morphologies of Au-coated AgNWs prepared using HAuCl<sub>4</sub>-only solution and the solution containing 50 mM NaCl are investigated. The HAuCl<sub>4</sub> solution without NaCl leads to the formation of particulate Au and results in severe AgNWs loss as shown in Fig. 2d, e, and Supplementary Fig. 6. This originates from the reaction stoichiometry and rapid electrochemical reaction rate. In contrast, the slower reaction induced by adding 50 mM NaCl to the HAuCl<sub>4</sub> solution results in galvanic replacement occurring primarily at the outer atoms of the AgNWs, as shown in Fig. 2f, g<sup>18</sup>. This leads to a predominantly uniform Au coating on the AgNWs and the

formation of partially hollow structured Au-coated AgNWs, which do not compromise the electrical properties (Supplementary Fig. 7).

#### Electrical properties of organic transistors based on Au-coated AgNWs/PDMS electrodes

We firstly investigated the  $R_C$  in organic transistors using Au-coated AgNWs/PDMS electrodes prepared by HAuCl<sub>4</sub> solutions containing various  $C_{\text{NaCl}}$ . Figure 3a illustrates the organic transistors, fabricated with PTB7-Th and ion gel as the organic semiconductor and gate dielectric, respectively<sup>27</sup>. In particular, PTB7-Th, selected for its significantly negative highest occupied molecular orbital (HOMO) level ( $E_{\text{HOMO}} = -5.24$  eV) compared to the Fermi level of silver<sup>28</sup>, highlights the substantial  $R_C$  in the organic transistor and exhibits clear  $R_C$  change depending on the morphologies of Au-coated AgNWs/PDMS (Fig. 3b, c). The detailed materials preparation and device fabrication process are described in the Experimental Section and schematically illustrated in Supplementary Fig. 8.

The  $R_C$  of the PTB7-Th based organic transistors based on Au-coated AgNWs/PDMS electrodes prepared by various  $C_{\text{NaCl}}$  in 0.5 mM HAuCl<sub>4</sub> solution for the galvanic replacement was investigated using the transfer length method (TLM)<sup>17</sup>. The channel length ( $L_{\text{CH}}$ ) of devices varied from 30 to 400  $\mu\text{m}$ , while the channel width ( $W_{\text{CH}}$ ) was fixed at 1250  $\mu\text{m}$ . The width-normalized ON resistances ( $R_{\text{ON}}W$ ) depending on  $L_{\text{CH}}$  of devices in different conditions are plotted in Supplementary Fig. 9, and  $R_C W$  for each condition is extracted from these plots. The details for TLM are described in Supplementary Note 1. As shown in Fig. 3d,  $R_C W$  of devices significantly decreased with 50 mM  $C_{\text{NaCl}}$  in the HAuCl<sub>4</sub> solution ( $387 \pm 72$   $\Omega\text{-cm}$ ) compared to devices using pristine AgNWs/PDMS electrode ( $849 \pm 162$   $\Omega\text{-cm}$ ) and those with Au coating from HAuCl<sub>4</sub>-only ( $655 \pm 147$   $\Omega\text{-cm}$ ) solution. Negligible  $R_C W$  change at higher  $C_{\text{NaCl}}$  suggests saturated Au coverage above  $C_{\text{NaCl}}$  of 50 mM, corresponding to the observed morphological trends. This result suggests that using NaCl-

containing  $\text{HAuCl}_4$  solution for the galvanic replacement of Au coating on AgNWs/PDMS could be an effective approach to enhance charge carrier transport between the soft electrode and the organic semiconductor.

We further evaluated the electrical characteristics of the device using Au-coated AgNWs/PDMS electrodes prepared by galvanic replacement with varying  $C_{\text{NaCl}}$ . For consistent comparison,  $L_{\text{CH}}$  and  $W_{\text{CH}}$  for all devices were fixed at 100 and 1250  $\mu\text{m}$ , respectively. The representative output characteristics of the organic transistors under different conditions are shown in Supplementary Fig. 10, where all devices exhibited typical *p*-channel behavior. The hysteresis behavior of the transistors presented in Supplementary Fig. 11 is comparable to that reported for ion-gated transistors<sup>29</sup>. As shown in Fig. 3e and Supplementary Fig. 12, obvious performance differences were observed in the devices made with the solutions containing varying  $C_{\text{NaCl}}$ . The ON current of the devices was clearly enhanced as the  $C_{\text{NaCl}}$  in the  $\text{HAuCl}_4$  solution increased and saturated from 50 mM of  $C_{\text{NaCl}}$ . The mobility ( $\mu_{\text{FE}}$ ), subthreshold swing (s.s.), and threshold voltage ( $V_{\text{TH}}$ ) of the transistors were extracted from the transfer curves as described in Supplementary Note 2. As plotted in Fig. 3f, the devices utilizing AgNWs/PDMS electrodes without and with Au coating (using  $C_{\text{NaCl}} = 0$  mM) showed the average  $\mu_{\text{FE}}$  of  $1.30 \pm 0.89$  and  $2.42 \pm 0.62 \text{ cm}^2 \cdot \text{V}^{-1} \cdot \text{s}^{-1}$ , respectively, while those using 50 mM  $C_{\text{NaCl}}$  achieved an average  $\mu_{\text{FE}}$  of  $7.45 \pm 0.64 \text{ cm}^2 \cdot \text{V}^{-1} \cdot \text{s}^{-1}$ . This  $\mu_{\text{FE}}$  trend correlates with  $R_{\text{C}}$  change. Furthermore, the subthreshold swing (s.s.) decreased from  $325.21 \pm 35.48 \text{ mV/dec}$  in devices with Au-coated AgNWs/PDMS electrodes prepared without NaCl to  $200.19 \pm 37.69 \text{ mV/dec}$  in those prepared with 50 mM  $C_{\text{NaCl}}$  (Supplementary Fig. 13a). This reduction is attributed to the enhanced charge carrier injection efficiency between the semiconductor and electrode, facilitated by uniform Au coating on AgNWs/PDMS by utilizing NaCl. However, as shown in Supplementary Fig. 13b, the threshold voltage ( $V_{\text{TH}}$ ) remained largely unchanged across devices, regardless of NaCl use. This is because of the inherently low operating voltage characteristic of the ion-gating operation in this organic transistor, which results in only minor and imperceptible variations in  $V_{\text{TH}}$ . Similar performance enhancements in  $\mu_{\text{FE}}$  were also observed in organic transistors based on another *p*-type organic semiconductor, poly(3-hexylthiophene-2,5-diyl) (P3HT), with a HOMO level of  $-5.0 \text{ eV}$ <sup>30</sup>, as shown in Supplementary Fig. 14. These results underscore the versatility of our approach for organic transistors with AgNWs/PDMS electrodes.

### Fully soft organic transistors

We demonstrated high-performance, fully soft organic transistors comprised entirely of soft materials, utilizing Au-coated AgNWs/PDMS electrodes prepared with a 0.5 mM  $\text{HAuCl}_4$  solution containing 50 mM NaCl. The soft electrode exhibits excellent robustness in its electrical characteristics under 80% mechanical strain with no obvious degradation of the Au coating, as shown in Supplementary Fig. 15. A polymer blend comprising PTB7-Th and PDMS, referred to as PTB7-Th/PDMS, was utilized as a soft organic semiconductor. This selection was driven by the significant performance degradation observed in transistors solely composed of PTB7-Th under a mechanical strain of 80%<sup>31</sup>. Numerous cases involving blends of polar semiconducting polymers and non-polymeric insulating polymers exhibit phase separation, a phenomenon known as the confinement effect. This effect results in the formation of a continuously connected semiconductor network, as schematically illustrated in Fig. 4a<sup>32</sup>. The atomic force microscopic (AFM) images reveal clear lateral phase separation in PTB7-Th/PDMS (Fig. 4b) compared to the uniformly dispersed phase in PTB7-Th (Supplementary Fig. 16). It is known that the morphology of the PTB7-Th/PDMS blend, which is induced by strong intermolecular interactions, is mainly influenced by the dipole moment and planarity of the semiconductor molecule<sup>32</sup>. Indeed, PTB7-Th has a considerably large dipole moment of 5.25 D (Fig. 4c), which was estimated using density functional theory (DFT). However, the dihedral angles between neighboring benzodithiophene and thieno[3,4-b]thiophene units, obtained at 27.67° and 15.22° (Supplementary Fig. 17), indicate relatively low planarity compared to semiconductors with reported high planarity<sup>32</sup>. This suggests that it is the

dipole moment, rather than the planarity, that primarily contributes to inducing confinement effects. It is noted that the DFT calculation employed the B3LYP/6-31 G (d,p) simulation model. This model was based on a dimer comprising two repeating units of the PTB7-Th backbone, where methyl groups were used instead of the bulky 2-ethylhexyl chains for simplification. The noticeable redshift of the 0–0 peak, along with the significant increase in the ratio of the 0–0 to 0–1 peaks in the UV-vis absorption spectrum of the PTB7-Th/PDMS film, indicates strong inter-chain  $\pi$ - $\pi$  interactions arising from the confinement effect (Supplementary Fig. 18)<sup>33</sup>.

The mechanical robustness of the PTB7-Th/PDMS film was confirmed by OM and AFM images. Both the pristine PTB7-Th and the PTB7-Th/PDMS films exhibit no obvious damage under a mechanical strain of up to 80%, as observed in the OM images (Fig. 4d and Supplementary Fig. 19a). However, as shown in the AFM images, the pristine PTB7-Th film exhibits visible microcracks under a strain greater than 50% (Supplementary Fig. 19b), whereas no cracks are observed in the PTB7-Th/PDMS film even at a strain of 80% (Fig. 4e). This resilience is attributed to the elastic domains absorbing strain and minimizing stress in the fibrous networks, as schematically illustrated in Supplementary Fig. 20<sup>34</sup>.

The representative output and transfer characteristics, as well as the hysteresis behavior of the fabricated fully soft transistor, using the PTB7-Th/PDMS blend, are shown in Supplementary Figs. 21 and 22, which features typical *p*-channel characteristics. The confinement effect in the soft semiconductor, combined with the low contact resistance between the semiconductor and the electrode, synergistically contributes to the high performance of the fully soft organic transistor. These transistors exhibit an average  $\mu_{\text{FE}}$  of  $13.09 \pm 4.17 \text{ cm}^2 \cdot \text{V}^{-1} \cdot \text{s}^{-1}$ , and the highest  $\mu_{\text{FE}}$  of  $21.87 \text{ cm}^2 \cdot \text{V}^{-1} \cdot \text{s}^{-1}$  (Fig. 4f, g), surpassing the mobilities of previously reported fully soft organic transistors (Fig. 4h)<sup>17,29,31,35-38</sup>. The representative electrical characteristics of the device under various mechanical strains (0%, 20%, 50%, 80%, and after release to 0%) demonstrated its reliable operation (Fig. 4i-k and Supplementary Fig. 23). Notably, no physical damage or severe performance degradation was observed, even at an 80% strain both along and perpendicular to the  $L_{\text{CH}}$  directions (Supplementary Fig. 24). It is worth mentioning that the  $\mu_{\text{FE}}$  was calculated by considering channel geometry change under the strains. Under the mechanical strains applied along the  $L_{\text{CH}}$  directions,  $\mu_{\text{FE}}$  and  $V_{\text{TH}}$  exhibited moderate changes from  $16.15 \text{ cm}^2 \cdot \text{V}^{-1} \cdot \text{s}^{-1}$  at 0% to  $11.51 \text{ cm}^2 \cdot \text{V}^{-1} \cdot \text{s}^{-1}$  at 80%, and from  $-2.33 \text{ V}$  to  $-2.20 \text{ V}$ , respectively. Upon completely releasing the mechanical strain, both the  $\mu_{\text{FE}}$  and  $V_{\text{TH}}$  returned to  $15.36 \text{ cm}^2 \cdot \text{V}^{-1} \cdot \text{s}^{-1}$  and  $-2.09 \text{ V}$ , respectively. In the case of the device under strain perpendicular to the  $L_{\text{CH}}$  direction, a similar trend was observed for both the  $\mu_{\text{FE}}$  ( $14.04 \text{ cm}^2 \cdot \text{V}^{-1} \cdot \text{s}^{-1}$  at 0%,  $7.42 \text{ cm}^2 \cdot \text{V}^{-1} \cdot \text{s}^{-1}$  at 80%, and  $13.01 \text{ cm}^2 \cdot \text{V}^{-1} \cdot \text{s}^{-1}$  at 0% released) and  $V_{\text{TH}}$  ( $-2.35 \text{ V}$  at 0%,  $-2.33 \text{ V}$  at 80%, and  $-2.36 \text{ V}$  at 0% released) as with the strain along the  $L_{\text{CH}}$  direction. To evaluate the durability of the fully soft transistor under mechanical stress, we further investigated its resistance to fatigue through repetitive stretching/releasing cycles of the device under a tensile strain of up to 80% in both along and perpendicular to the  $L_{\text{CH}}$  direction. Figure 4l, m and Supplementary Fig. 25 show the representative transfer characteristics of the devices after 1000 cycles of stretching/releasing to an 80% strain, which notably demonstrated no significant performance degradation. Importantly,  $\mu_{\text{FE}}$  and  $V_{\text{TH}}$  showed only minor changes;  $\mu_{\text{FE}}$  decreased from  $14.15 \text{ cm}^2 \cdot \text{V}^{-1} \cdot \text{s}^{-1}$  to  $10.05 \text{ cm}^2 \cdot \text{V}^{-1} \cdot \text{s}^{-1}$ , and  $V_{\text{TH}}$  shifted from  $-2.10 \text{ V}$  to  $-2.24 \text{ V}$ , following 1000 cycles of stretching/releasing along the  $L_{\text{CH}}$  direction. Additionally, a similar trend was observed for cyclic stretching perpendicular to the  $L_{\text{CH}}$  direction:  $\mu_{\text{FE}}$  was changed from  $13.18 \text{ cm}^2 \cdot \text{V}^{-1} \cdot \text{s}^{-1}$  to  $8.54 \text{ cm}^2 \cdot \text{V}^{-1} \cdot \text{s}^{-1}$  and  $V_{\text{TH}}$  from  $-2.36 \text{ V}$  to  $-2.31 \text{ V}$  after 1000 cycles. These results confirm the robust mechanical durability of the devices, maintaining their functional stability through extensive stress cycles. Supplementary Figure 26 presents the fully soft transistor undergoing various mechanical deformations, including stretching, bending, and twisting, exhibiting its adaptability. The use of all elastomeric materials in the devices ensures that the fully soft transistor can be deformed readily without sustaining physical damage. These results indicate that our

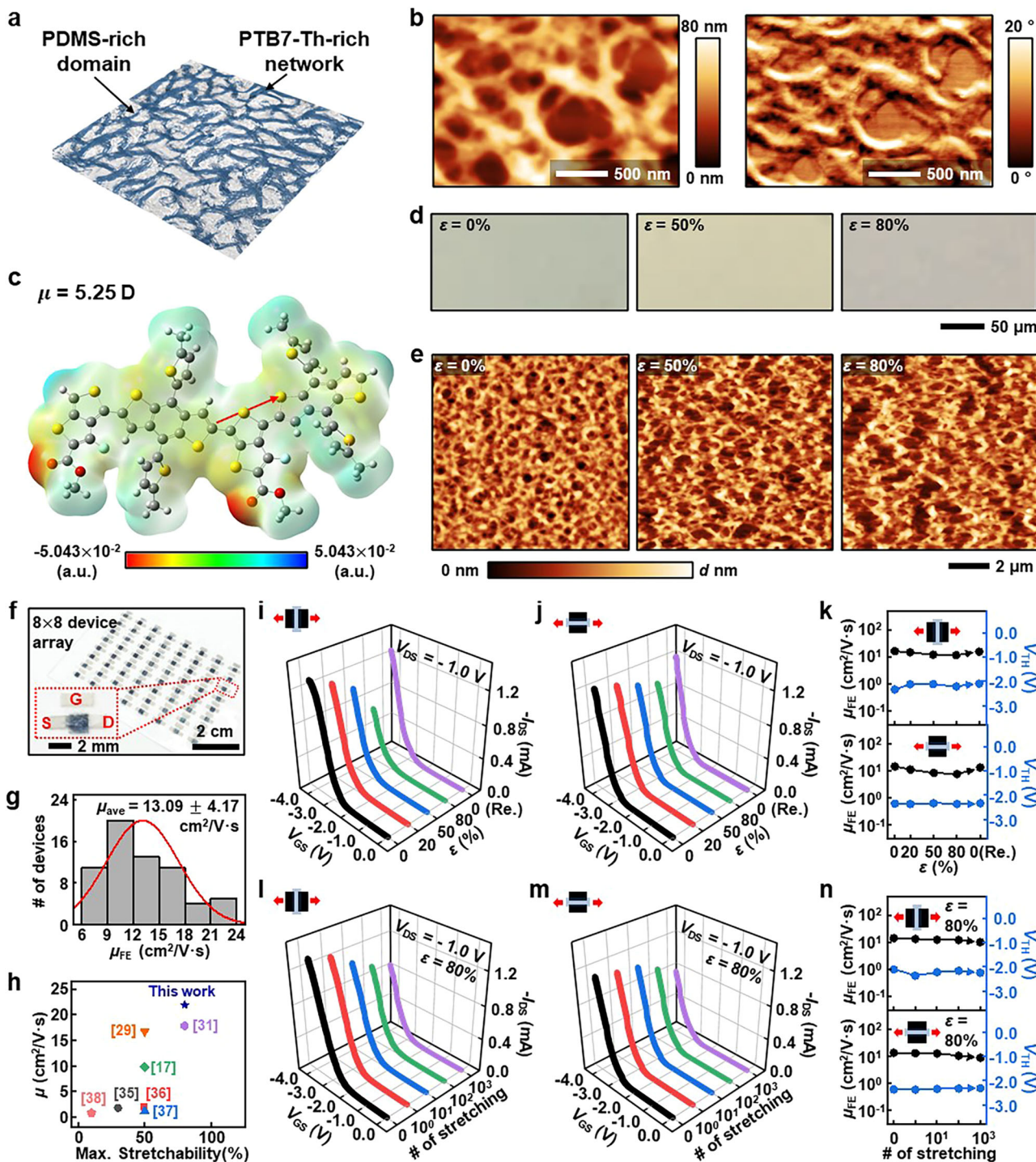


**Fig. 4 | High-performance fully soft organic transistors.** **a** Schematic of the soft semiconducting PTB7-Th/PDMS composite. **b** AFM images of the PTB7-Th/PDMS composites in the height (left), and phase (right) modes. **c** Molecular electrostatic potential map and the dipole moment of the PTB7-Th. Sequential optical (d), and AFM height (e) images of the PTB7-Th under the various mechanical strains. Note that  $d$  is 190, 220, 250 nm from the left in (e). **f** An optical image of the  $8 \times 8$  fully soft organic transistors array. Inset is the magnified optical image of a single device. **g** The  $\mu_{FE}$  distribution of the high-performance fully soft organic transistors. Data are presented as mean values  $\pm$  1 s.d. based on measurements from 64 devices.

The comparison of the  $\mu$  and maximum stretchability with the reported fully soft organic transistors. Transfer characteristics of the fully soft organic transistors under the strains parallel (i), and perpendicular (j) to the channel length direction. **k**  $\mu_{FE}$  and  $V_{TH}$  changes of the fully soft organic transistors under the strains parallel (top), and perpendicular (bottom) to the channel length direction. Transfer characteristics of the fully soft organic transistors after the repetitive strains parallel (l), and perpendicular (m) to the channel length direction. **n**  $\mu_{FE}$  and  $V_{TH}$  changes of the fully soft organic transistors after the repetitive strains parallel (top), and perpendicular (bottom) to the channel length direction.

approach, involving the addition of NaCl to the HAuCl<sub>4</sub> solution for effective coating of the exposed AgNWs of the AgNWs/PDMS electrodes, provides a practical means to realize high-performance fully soft electronics.

### Soft glucose sensors

Mechanical softness and chemical inertness are essential for bio-implantable devices<sup>39,40</sup>. Although the AgNWs/PDMS electrode has been employed in various bioelectronics<sup>5,41</sup>, its inherent vulnerability to chemical

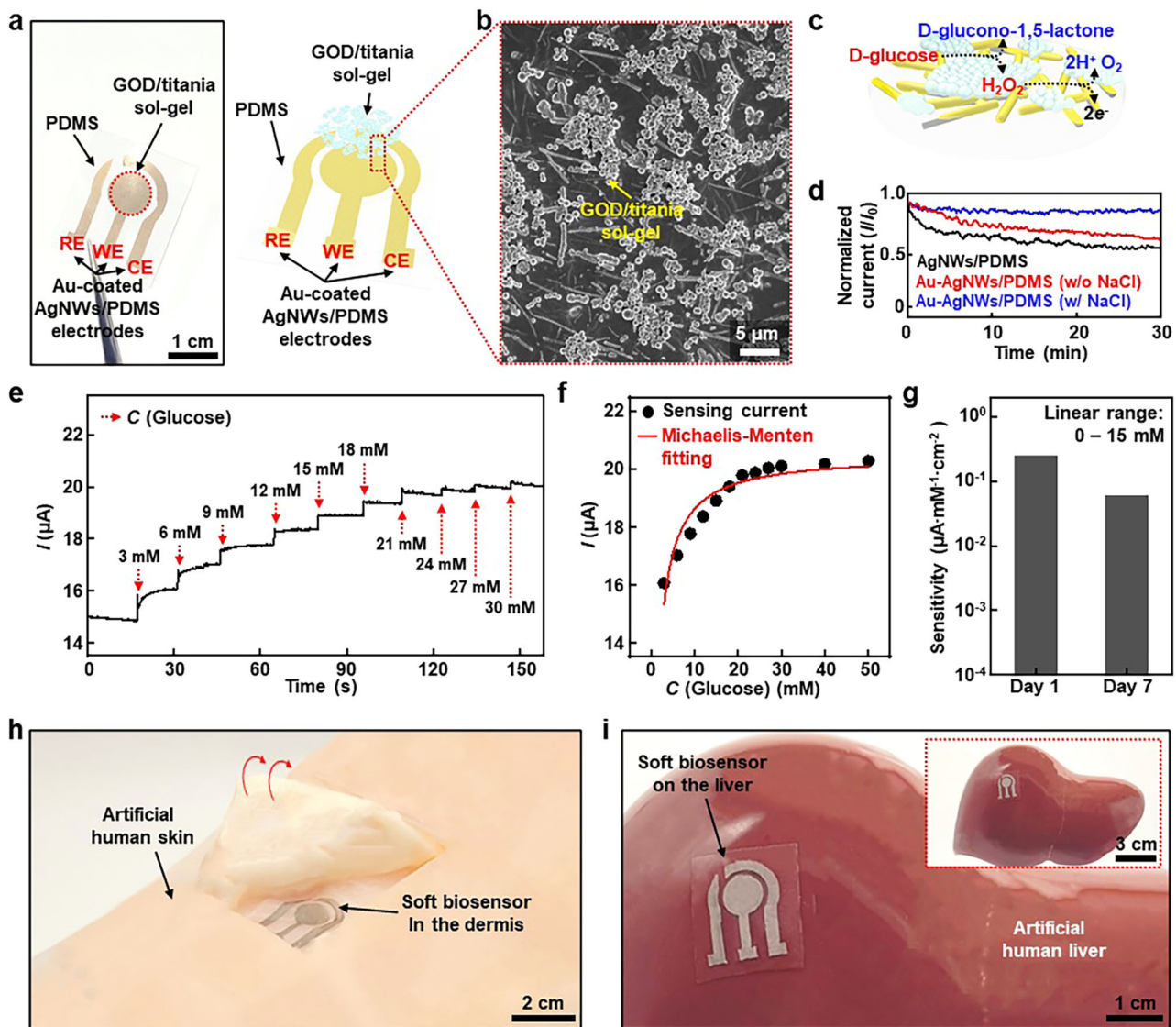


**Fig. 5 | Soft glucose sensors.** **a** An optical image (left), and schematic exploded view (right) of the soft glucose sensors based on Au-coated AgNWs/PDMS electrodes galvanic replaced with 50 mM NaCl containing 0.5 mM HAuCl<sub>4</sub> solution. **b** SEM image of the sensing area on the working electrode. **c** Schematic sensing mechanism of the glucose sensors. **d** Electrochemical stability of the AgNWs/PDMS and Au-coated AgNWs/PDMS electrodes in a 30 mM H<sub>2</sub>O<sub>2</sub> solution.

**e** Chronoamperometric current response of the soft glucose sensor at different glucose concentrations. **f** Calibration curve of the soft glucose sensor with a Michaelis-Menten model-based fitting curve. **g** Sensitivity of the soft glucose sensors. Optical images of the soft glucose sensors applicable as bio-implantable devices in the dermis (**h**), and on the liver (**i**). Inset in the (**i**) is the optical image without magnification.

oxidation presents challenges for broader application. Specifically, implantable glucose sensors with a soft format, which monitor glucose concentrations in interstitial fluids, offer significant advantages for diabetes management due to the high correlation between blood and interstitial fluid glucose levels<sup>42</sup>. AgNWs/PDMS electrodes, while promising and useful, are not ideal for soft glucose sensors. This is because typical glucose sensors are enzymatic and involve the generation of H<sub>2</sub>O<sub>2</sub> during glucose detection<sup>43</sup>, which adversely affects the stability of the AgNWs<sup>44</sup>. Therefore, our approach for the complete Au coating on the exposed AgNWs of the AgNWs/PDMS electrode significantly enhances its resistance to severe oxidation.

The soft glucose sensors were fabricated using uniformly Au-coated AgNWs/PDMS electrodes, prepared through galvanic replacement with HAuCl<sub>4</sub> containing 50 mM NaCl. The sensor comprised an enzymatic sensing membrane and three electrodes: a working electrode (WE), a counter electrode (CE), and a reference electrode (RE) (Fig. 5a). Glucose oxidase (GOD) was used for the sensing membrane due to its specificity and stability<sup>45,46</sup>. The GOD layer was immobilized on the sensing electrode via

hydrolysis with GOD and titanium isoperoxide, forming a particulate morphology similar to previous studies (Fig. 5b)<sup>45</sup>. EDX elemental mapping confirmed the well-formed GOD-titania sol-gel film (Supplementary Fig. 27). The detailed fabrication process of soft glucose sensors is described in the Experimental section. Immobilized GOD on the electrode accelerates D-glucose dissociation, generating H<sub>2</sub>O<sub>2</sub>, and consequently, electrons. Thus, the current measured by the sensor is determined by glucose concentration, as schematically illustrated in Fig. 5c and specifically described in Supplementary Note 3.

The complete Au coating on the exposed AgNWs of the AgNWs/PDMS electrode, prepared using HAuCl<sub>4</sub> containing NaCl, offers excellent electrochemical inertness. This property is crucial in oxidative environments, such as those involving H<sub>2</sub>O<sub>2</sub>. While AgNWs/PDMS electrodes show stability in mild environments (e.g., phosphate-buffered saline; PBS) (Supplementary Fig. 28), they are vulnerable to oxidation in oxidizing conditions. Figure 5d shows dramatic decrease in current flow for pristine AgNWs/PDMS under a 400 mV applied voltage in a 30 mM H<sub>2</sub>O<sub>2</sub> solution. In contrast, electrodes with particulate Au coatings, prepared using HAuCl<sub>4</sub>

without NaCl, show a decline in current over time. However, those with a complete Au coating, prepared with NaCl in the HAuCl<sub>4</sub> solution, exhibit negligible change. This stability is attributed to the prevention of electrochemical etching of Ag by H<sub>2</sub>O<sub>2</sub> (Supplementary Fig. 29), indicating that complete Au coating on AgNWs/PDMS maintains electrical performance even in oxidative environments. Therefore, complete Au-coated AgNWs/PDMS represents an effective approach for enzyme-based soft glucose sensors.

A constant potential of 400 mV was applied to RE for chronamperometric measurement of the glucose sensor across glucose concentrations ranging from 0 to 30 mM. This range adequately covers the normal and diabetic glucose levels in human interstitial fluid (approximately 2 to 23 mM)<sup>47</sup>. Figure 5e clearly shows the current response of the sensor to various glucose concentrations. Within the 0 to 15 mM range, the sensor exhibits a linear relationship between glucose concentration and measured current, with a sensitivity of 0.238  $\mu\text{A} \cdot \text{mM}^{-1} \cdot \text{cm}^{-2}$ , and the limit of detection (LOD) of 0.498 mM (Supplementary Fig. 30, and Supplementary Note 4). Such sensing performance significantly outperforms that of the soft glucose sensor fabricated using an Au-coated AgNWs/PDMS electrode prepared via galvanic replacement without NaCl. In particular, the non-uniform Au coating exposes AgNWs to H<sub>2</sub>O<sub>2</sub>, leading to electrochemical degradation of the electrode, which results in unstable sensing capability and a low sensitivity of 0.168  $\mu\text{A} \cdot \text{mM}^{-1} \cdot \text{cm}^{-2}$  (Supplementary Fig. 31). The current response of the soft glucose sensor with uniformly Au-coated AgNWs/PDMS electrode, extending up to 50 mM was fitted using the Michaelis-Menten Kinetic model (Fig. 5f)<sup>48</sup>. The Michaelis-Menten constant ( $K_M$ ) and maximum current ( $I_{\text{MAX}}$ ) were 0.914 mM and 20.35  $\mu\text{A}$ , respectively, as extracted from the Lineweaver-Burk plot (Supplementary Fig. 32). The detailed information is described in Supplementary Note 5. The sensor reliably maintains its sensing capability after seven days in PBS, as shown in Fig. 5g. This stability is attributed to the enhanced inertness provided by the complete Au coating on the electrode. Besides inertness, mechanical softness is a crucial attribute of our devices. Supplementary Fig. 33 shows the durability of the devices under various mechanical deformations, including bending and stretching. With these key features of inertness and softness, as well as biocompatibility of components<sup>49-51</sup>, the device exhibits significant potential as a bio-implantable solution. The successful conceptual demonstration of its conformal implantation both in the dermis and on the liver (Fig. 5h, i) underscores the ability of our work to address critical challenges, positioning it as a promising candidate for future bio-implantable devices.

## Discussion

In this study, we have demonstrated a simple, effective, and reliable method for gold coating on AgNWs/PDMS electrodes, significantly advancing the field of soft electronics, including transistors and glucose sensors. We achieved uniform and complete Au coating on the exposed AgNWs of AgNWs/PDMS electrodes through galvanic replacement, facilitated by the addition of NaCl to the HAuCl<sub>4</sub> solution. While a vigorous reaction with HAuCl<sub>4</sub> solution leads to a non-uniform and particulate Au coating on the surface of AgNWs, adding NaCl to the HAuCl<sub>4</sub> results in a uniform and complete Au coating. This is achieved by a slower reaction, which is a result of Le Chatelier's principle and the change in reduction potential, coupled with the prevention of AgCl precipitation due to the presence of excess Cl<sup>-</sup>. The uniform Au coating on the AgNW/PDMS electrodes significantly reduced  $R_C$  with the organic semiconductor in PTB7-Th based organic transistors, thereby remarkably enhancing the electrical performance of these devices. Furthermore, the development of fully soft organic transistors with decreased  $R_C$  and enhanced stretchability of PTB7-Th/PDMS highlights the potential of our approach in creating high-performance fully soft organic electronics. These advancements promise not only to revolutionize wearable technology but also to open new avenues in bio-implantable healthcare systems. The demonstrated soft glucose sensors, empowered by our complete Au-coated AgNWs/PDMS electrodes, exhibit significant electrochemical stability, paving the way for future bio-implantable devices.

## Methods

### Materials

Poly[4,8-bis(5-(2-ethylhexyl) thiophen-2-yl) benzo[1,2-b;4,5-b']dithiophene-2,6-diyl-alt-(4-(2-ethylhexyl)-3-fluorothieno[3,4-b]thiophene)-2-carboxylate-2,6-diyl] (PTB7-Th) was synthesized as previously reported<sup>31</sup>. Chloroform (>99%), gold chloride trihydrate (HAuCl<sub>4</sub>·3H<sub>2</sub>O; >99.9%), 1-Ethyl-3-methylimidazolium bis(trifluoromethylsulfonyl)imide (EMIM-TFSI), poly(vinylidene fluoride-co-hexafluoropropylene) (PVDF-co-HFP; molecular weight = ~400,000), poly(3-hexylthiophene-2,5-diyl) (P3HT; molecular weight = 50,000–100,000), D-(+)-glucose, glucose oxidase (GOD) from Aspergillus niger (Type X-S; 100,000–250,000 units/g solid), were purchased from Sigma-Aldrich, and used as received. Ammonia (NH<sub>4</sub>OH; 25.0–29.0%) was purchased from Duksan Chemicals. Acetone was purchased from Samchun Chemicals. Silver nanowires (AgNWs) solution (average diameter = 75–105 nm, average length = 40–80  $\mu\text{m}$ , 1 wt% in IPA) was purchased from Kechuang. Polydimethylsiloxane (PDMS; Sylgard 184 silicone elastomer kit) was purchased from Dow-Corning. Titanium isopropoxide (98%) was purchased from Daejung Chemicals & Metals. Phosphate-Buffered Saline (10X, pH = 7.4) (PBS) was purchased from Invitrogen, which was diluted 10 times with ultra-pure water (CBW012) purchased from Dyne Bio for the experiment before use.

### Preparation of AgNWs/PDMS electrode

For the preparation of the AgNWs/PDMS electrodes, the AgNWs were patterned by dropping AgNWs solution on a glass substrate with a polyimide tape-based shadow mask prepared by a programmable cutting machine (Silhouette Portrait 3), followed by drying at 60 °C for 10 min. Then, the shadow mask was detached from the substrate, and the patterned AgNWs were annealed at 200 °C for 20 min, which induced conductivity improvement. The channels were formed with razor blades subsequently for the fabrication of the organic transistors. Next, the degassed liquid phase PDMS (10:1 (w/w) pre-polymer/curing agent) was applied onto the patterned AgNWs by spin-casting at 250 rpm for 60 s, then solidified at 100 °C for 1 h. Due to the porous nature of the AgNWs network, liquid-phase PDMS can penetrate the pores of the networks, resulting in partially embedded AgNWs in PDMS. The solidified PDMS film was then carefully peeled off from the glass substrate to complete the preparation of AgNWs/PDMS electrodes.

### Galvanic replacement process

The exposed AgNWs of AgNWs/PDMS electrodes were coated with Au by galvanic replacement. For the galvanic replacement, 0.5 mM HAuCl<sub>4</sub> solutions containing different C<sub>NaCl</sub> (0, 10, 20, 50, 100, 200 mM) were used. The prepared solution was dropped on the desired area of the AgNWs/PDMS electrode, specifically on the channels, followed by keeping the sample at room temperature for various periods. Then, the Au-coated AgNWs/PDMS electrodes were rinsed with DI water and immersed in NH<sub>4</sub>OH for 1 min to remove the byproducts, AgCl, formed during the galvanic replacement. Finally, the fabrication of Au-coated AgNWs/PDMS electrodes was completed by washing with DI water, followed by blowing the remaining water away with N<sub>2</sub> and dehydration at 90 °C for 10 min.

### Preparation of organic semiconductor solution

The PTB7-Th solution was prepared by dissolving PTB7-Th in the chloroform (3 mg/ml) at 80 °C for 20 min. The P3HT solution was prepared by dissolving P3HT in the chloroform (5 mg/ml) at 60 °C for 20 min. The prepared PTB7-Th and P3HT solutions were used to fabricate the transistor to analyze various electrical characteristics. In the case of preparation of soft organic semiconductor solution, prepared 3 mg/ml PTB7-Th solution was blended with liquid-phase PDMS solution (10:1 (w/w) pre-polymer/curing agent, 0.12 g/ml in chloroform) in a volume ratio of 10:1. The weight ratio between PTB7-Th and PDMS was 1:4 in the resultant solution.

## Preparation of ion gel

To prepare ion gel dielectric, PVDF-co-HFP, dehydrated EMIM-TFSI, and acetone were mixed in a weight ratio of 1:4:7, followed by heating at 90 °C for 30 min. The homogeneously blended solution was dropped onto the cleaned glass substrate and solidified at 70 °C for 12 h in a vacuum oven. The solidified ion gel was cut into the desired shape using a razor blade.

## Organic transistor fabrication

The fabrication of the transistors began with preparing patterned Au-coated AgNWs/PDMS electrodes. Then, PTB7-Th, P3HT, or PTB7-Th/PDMS was patterned by spin-casting (1500 rpm, 30 s) on the channel area of the electrodes with polyimide film-based shadow mask, followed by annealing of the sample at 120 °C for 20 min. It is noted that the retention time of the solution on the substrate before spin-casting is no longer than 1 s, which prevents swelling of the substrate by the solvent, chloroform. This short retention time, combined with the high volatility of chloroform and rapid spin speed, ensures the formation of a high-quality semiconducting film. Then, the prepared ion gel was laminated on top of the organic semiconductor and gate electrode to complete device fabrication.

## Glucose sensor fabrication

The fabrication of the glucose sensors began with the preparation of patterned electrodes, Au-coated AgNWs/PDMS, using NaCl contained HAuCl<sub>4</sub> solution for uniform Au coating. Following this, a pre-prepared solution of glucose oxidase (GOD) at a concentration of 10 mg/ml in PBS was delicately applied to the working electrode. To immobilize the GOD onto the electrode, the working electrode area was consistently exposed to a vapor of titanium isopropoxide solution for 8 h at room temperature. After this immobilization step, the sensor was thoroughly rinsed with ultrapure water to complete the fabrication process. The resulting glucose sensors were then stored in PBS at 4 °C, both before and after their characterization. This storage protocol ensures the stability and readiness of the sensors for subsequent analytical procedures.

## Characterization

The cyclic voltammograms were obtained using a potentiostat (CHI 604E, CH Instruments) with three electrodes, including 3 mm glassy carbon, Pt wire, and Ag/AgCl (3 M NaCl) as working, counter, and reference electrodes, respectively. The surface morphologies, elemental mapping of AgNWs/PDMS electrodes, Au-coated AgNWs/PDMS electrodes, and GOD/titania were characterized by field emission scanning microscopy (SU7000, Hitachi) equipped with energy dispersive X-ray spectroscopy (EDAX element EDS system, Ametek). Atomic force microscopy (XE-100, Park Systems) was used to investigate the surface morphologies of organic semiconductors. The absorption spectra of the organic semiconductor film were obtained by spectrophotometer (V-670, JASCO). All the electrical performances were characterized by a semiconductor analyzer (4200-SCS, Keithley Instruments) with a probe station (MST 8000 C, MS Tech). The customized stretcher was additionally used for measuring device performance under mechanical strain.

## Data availability

The data that support the plots within this paper and other findings of this study are available from the corresponding author upon reasonable request.

Received: 20 May 2024; Accepted: 18 September 2024;

Published online: 04 October 2024

## References

- Ray, T. R. et al. Bio-Integrated Wearable Systems: A Comprehensive Review. *Chem. Rev.* **119**, 5461–5533 (2019).
- Song, Y., Min, J. & Gao, W. Wearable and Implantable Electronics: Moving toward Precision Therapy. *ACS Nano* **13**, 12280–12286 (2019).
- Sim, K., Rao, Z., Ershad, F. & Yu, C. Rubbery Electronics Fully Made of Stretchable Elastomeric Electronic Materials. *Adv. Mater.* **32**, 1902417 (2020).
- Iqbal, S. M. A., Mahgoub, I., Du, E., Leavitt, M. A. & Asghar, W. Advances in healthcare wearable devices. *npj Flex. Electron.* **5**, 9 (2021).
- Sim, K. et al. An epicardial bioelectronic patch made from soft rubbery materials and capable of spatiotemporal mapping of electrophysiological activity. *Nat. Electron.* **3**, 775–784 (2020).
- Li, Y., Li, N., De Oliveira, N. & Wang, S. Implantable bioelectronics toward long-term stability and sustainability. *Mater.* **4**, 1125–1141 (2021).
- Oh, J. Y. et al. Intrinsically stretchable and healable semiconducting polymer for organic transistors. *Nature* **539**, 411–415 (2016).
- Lampert, Z. A. et al. A simple and robust approach to reducing contact resistance in organic transistors. *Nat. Commun.* **9**, 5130 (2018).
- Waldrup, M., Jurchescu, O. D., Gundlach, D. J. & Bittle, E. G. Contact Resistance in Organic Field-Effect Transistors: Conquering the Barrier. *Adv. Funct. Mater.* **30**, 1904576 (2019).
- Borchert, J. W., Weitz, R. T., Ludwigs, S. & Klauk, H. A Critical Outlook for the Pursuit of Lower Contact Resistance in Organic Transistors. *Adv. Mater.* **34**, 2104075 (2022).
- Peng, B. et al. Crystallized Monolayer Semiconductor for Ohmic Contact Resistance, High Intrinsic Gain, and High Current Density. *Adv. Mater.* **32**, 2002281 (2020).
- Yamamura, A. et al. High-Speed Organic Single-Crystal Transistor Responding to Very High Frequency Band. *Adv. Funct. Mater.* **30**, 1909501 (2020).
- Kim, B., Choi, S. H., Zhu, X. Y. & Frisbie, C. D. Molecular tunnel junctions based on pi-conjugated oligoacene thiols and dithiols between Ag, Au, and Pt contacts: effect of surface linking group and metal work function. *J. Am. Chem. Soc.* **133**, 19864–19877 (2011).
- Dong, H., Wang, C. & Hu, W. High performance organic semiconductors for field-effect transistors. *Chem. Commun.* **46**, 5211–5222 (2010).
- Wang, Y. et al. Van der Waals contacts between three-dimensional metals and two-dimensional semiconductors. *Nature* **568**, 70–74 (2019).
- Kim, H. J., Sim, K., Thukral, A. & Yu, C. J. Rubbery electronics and sensors from intrinsically stretchable elastomeric composites of semiconductors and conductors. *Sci. Adv.* **3**, e1701114 (2017).
- Sim, K. et al. Fully rubbery integrated electronics from high effective mobility intrinsically stretchable semiconductors. *Sci. Adv.* **5**, eaav5749 (2019).
- Kim, T. et al. Highly transparent Au-coated Ag nanowire transparent electrode with reduction in haze. *ACS Appl. Mater. Interfaces* **6**, 13527–13534 (2014).
- El Mel, A.-A. et al. Galvanic Replacement Reaction: A Route to Highly Ordered Bimetallic Nanotubes. *J. Phys. Chem. C* **120**, 17652–17659 (2016).
- Wang, Y. et al. Highly stable, stretchable, and transparent electrodes based on dual-headed Ag@Au core-sheath nanomatchsticks for non-enzymatic glucose biosensor. *Nano Res.* **16**, 1558–1567 (2022).
- Verma, N. A green synthetic approach for size tunable nanoporous gold nanoparticles and its glucose sensing application. *Appl. Surf. Sci.* **462**, 753–759 (2018).
- Chen, A. N., McClain, S. M., House, S. D., Yang, J. C. & Skrabalak, S. E. Mechanistic Study of Galvanic Replacement of Chemically Heterogeneous Templates. *Chem. Mater.* **31**, 1344–1351 (2019).
- Chee, S. W., Tan, S. F., Baraissov, Z., Bosman, M. & Mirsaidov, U. Direct observation of the nanoscale Kirkendall effect during galvanic replacement reactions. *Nat. Commun.* **8**, 1224 (2017).
- Nehra, K. & Kumar, P. S. Chloride ion refined galvanic replacement: Boosting monodispersity of Au-Ag hollow nanoparticles & their enhanced applications. *Curr. Appl. Phys.* **18**, 1158–1170 (2018).

25. Kang, S. et al. Reducing Agent-Assisted Excessive Galvanic Replacement Mediated Seed-Mediated Synthesis of Porous Gold Nanoplates and Highly Efficient Gene-Thermo Cancer Therapy. *ACS Appl. Mater. Interfaces* **9**, 35268–35278 (2017).

26. Gogoi, S. K., Borah, S. M., Dey, K. K., Paul, A. & Chattopadhyay, A. Optically definable reaction-diffusion-driven pattern generation of Ag-Au nanoparticles on templated surfaces. *Langmuir* **27**, 12263–12269 (2011).

27. Lee, K. H. et al. Cut and stick" rubbery ion gels as high capacitance gate dielectrics. *Adv. Mater.* **24**, 4457–4462 (2012).

28. Arildii, D. et al. Highly Sensitive and Durable Organic Photodiodes Based on Long-Term Storable NiO(x) Nanoparticles. *ACS Appl. Mater. Interfaces* **14**, 14410–14421 (2022).

29. Guan, Y. S. et al. Air/water interfacial assembled rubbery semiconducting nanofilm for fully rubbery integrated electronics. *Sci. Adv.* **6**, eabb3656 (2020).

30. Zhang, Y., Chen, L., Hu, X., Zhang, L. & Chen, Y. Low Work-function Poly(3,4-ethylenedioxylenethiophene): Poly(styrene sulfonate) as Electron-transport Layer for High-efficient and Stable Polymer Solar Cells. *Sci. Rep.* **5**, 12839 (2015).

31. Park, D. H. et al. Highly Stretchable, High-Mobility, Free-Standing All-Organic Transistors Modulated by Solid-State Elastomer Electrolytes. *Adv. Funct. Mater.* **29**, 1808909 (2019).

32. Park, B. et al. Direct Observation of Confinement Effects of Semiconducting Polymers in Polymer Blend Electronic Systems. *Adv. Sci.* **8**, 2100332 (2021).

33. Xu, J. et al. Multi-scale ordering in highly stretchable polymer semiconducting films. *Nat. Mater.* **18**, 594–601 (2019).

34. Shin, M. et al. Polythiophene nanofibril bundles surface-embedded in elastomer: a route to a highly stretchable active channel layer. *Adv. Mater.* **27**, 1255–1261 (2015).

35. Rao, Z. et al. All-Polymer Based Stretchable Rubbery Electronics and Sensors. *Adv. Funct. Mater.* **32**, 2111232 (2021).

36. Lee, W., Kim, Y., Lee, M. Y., Oh, J. H. & Lee, J. U. Highly stretchable fiber transistors with all-stretchable electronic components and graphene hybrid electrodes. *Org. Electron.* **69**, 320–328 (2019).

37. Guan, Y.-S. et al. Elastic electronics based on micromesh-structured rubbery semiconductor films. *Nat. Electron.* **5**, 881–892 (2022).

38. Hong, K., Choo, D. H., Lee, H. J., Park, J. Y. & Lee, J. L. Substrate-free, stretchable electrolyte gated transistors. *Org. Electron.* **87**, 105936 (2020).

39. Zhai, Q. & Cheng, W. Soft and stretchable electrochemical biosensors. *Mater. Today Nano* **7**, 100041 (2019).

40. Kutbee, A. T. et al. Flexible and biocompatible high-performance solid-state micro-battery for implantable orthodontic system. *npj Flex. Electron.* **1**, 7 (2017).

41. Xu, G. et al. Battery-Free and Wireless Epidermal Electrochemical System with All-Printed Stretchable Electrode Array for Multiplexed In Situ Sweat Analysis. *Adv. Mater. Technol.* **4**, 1800658 (2019).

42. Kim, J. et al. Simultaneous Monitoring of Sweat and Interstitial Fluid Using a Single Wearable Biosensor Platform. *Adv. Sci.* **5**, 1800880 (2018).

43. Lee, H., Hong, Y. J., Baik, S., Hyeon, T. & Kim, D. H. Enzyme-Based Glucose Sensor: From Invasive to Wearable Device. *Adv. Healthc. Mater.* **7**, 1701150 (2018).

44. Sigg, L. & Lindauer, U. Silver nanoparticle dissolution in the presence of ligands and of hydrogen peroxide. *Environ. Pollut.* **206**, 582–587 (2015).

45. Yu, J., Liu, S. & Ju, H. Glucose sensor for flow injection analysis of serum glucose based on immobilization of glucose oxidase in titania sol-gel membrane. *Biosens. Bioelectron.* **19**, 401–409 (2003).

46. Yao, H., Shum, A. J., Cowan, M., Lahdesmaki, I. & Parviz, B. A. A contact lens with embedded sensor for monitoring tear glucose level. *Biosens. Bioelectron.* **26**, 3290–3296 (2011).

47. Bruen, D., Delaney, C., Florea, L. & Diamond, D. Glucose Sensing for Diabetes Monitoring: Recent Developments. *Sensors* **17**, 1866 (2017).

48. Sim, K. et al. Three-dimensional curvy electronics created using conformal additive stamp printing. *Nat. Electron.* **2**, 471–479 (2019).

49. Jiang, Z. et al. A 1.3-micrometre-thick elastic conductor for seamless on-skin and implantable sensors. *Nat. Electron.* **5**, 784–793 (2022).

50. Choi, S. et al. Highly conductive, stretchable and biocompatible Ag-Au core-sheath nanowire composite for wearable and implantable bioelectronics. *Nat. Nanotechnol.* **13**, 1048–1056 (2018).

51. Keum, D. et al. Wireless smart contact lens for diabetic diagnosis and therapy. *Sci. Adv.* **6**, eaba3252 (2020).

## Acknowledgements

This work was supported by the National Research Foundation of Korea (NRF) grant funded by the Korean government, Ministry of Science and ICT (NRF-2021R1C1C1007714, NRF-2023R1A2C3006550, and RS-2024-00346943). This work was also supported by the KRICT projects (KS2441-10, BSK24-125) from the Korea Research Institute of Chemical Technology.

## Author contributions

H.P. and K.S. conceived and designed the experiment. H.P., S.K., J.L., K.K., H.N., Y.K., and D.K. performed the experiments. H.P. and S.K. performed DFT calculations. K.K. synthesized organic semiconductors. H.P., S.K., J.L., K.K., H.N., Y.K., and D.S. analyzed the data. H.C. and K.S. wrote the manuscript. H.C., H.N., B.K., and K.S. reviewed and revised manuscript.

## Competing interests

The authors declare no competing interests.

## Additional information

**Supplementary information** The online version contains supplementary material available at <https://doi.org/10.1038/s41528-024-00349-5>.

**Correspondence** and requests for materials should be addressed to Kyoseung Sim.

**Reprints and permissions information** is available at <http://www.nature.com/reprints>

**Publisher's note** Springer Nature remains neutral with regard to jurisdictional claims in published maps and institutional affiliations.

**Open Access** This article is licensed under a Creative Commons Attribution-NonCommercial-NoDerivatives 4.0 International License, which permits any non-commercial use, sharing, distribution and reproduction in any medium or format, as long as you give appropriate credit to the original author(s) and the source, provide a link to the Creative Commons licence, and indicate if you modified the licensed material. You do not have permission under this licence to share adapted material derived from this article or parts of it. The images or other third party material in this article are included in the article's Creative Commons licence, unless indicated otherwise in a credit line to the material. If material is not included in the article's Creative Commons licence and your intended use is not permitted by statutory regulation or exceeds the permitted use, you will need to obtain permission directly from the copyright holder. To view a copy of this licence, visit <http://creativecommons.org/licenses/by-nc-nd/4.0/>.